# Measurement-Based Analysis, Modeling, and Synthesis of the Internet Delay Space[*]

Bo Zhang[†], T. S. Eugene Ng[†], Animesh Nandi[†‡], Rudolf Riedi[†], Peter Druschel[‡], Guohui Wang[†]
[†]Rice University, USA [‡]Max Planck Institute for Software Systems, Germany

## ABSTRACT

Understanding the characteristics of the Internet delay space (i.e., the all-pairs set of static round-trip propagation delays among edge networks in the Internet) is important for the design of global-scale distributed systems. For instance, algorithms used in overlay networks are often sensitive to violations of the triangle inequality and to the growth properties within the Internet delay space. Since designers of distributed systems often rely on simulation and emulation to study design alternatives, they need a realistic model of the Internet delay space.

Our analysis shows that existing models do not adequately capture important properties of the Internet delay space. In this paper, we analyze measured delays among thousands of Internet edge networks and identify key properties that are important for distributed system design. Furthermore, we derive a simple model of the Internet delay space based on our analytical findings. This model preserves the relevant metrics far better than existing models, allows for a compact representation, and can be used to synthesize delay data for simulations and emulations at a scale where direct measurement and storage are impractical.

## Categories and Subject Descriptors

C.2.m [**Computer-Communication Networks**]: Miscellaneous

## General Terms

Measurement, Performance, Experimentation

## Keywords

Internet delay space, measurement, analysis, modeling, synthesis, distributed system, simulation

[*]This research was sponsored by the NSF under CAREER Award CNS-0448546, and by the Texas Advanced Research Program under grant No.003604-0078-2003. Views and conclusions contained in this document are those of the authors and should not be interpreted as representing the official policies, either expressed or implied, of NSF, the state of Texas, or the U.S. government.

## 1. INTRODUCTION

Designers of large-scale distributed systems rely on simulation and network emulation to study design alternatives and evaluate prototype systems at scale and prior to deployment. To obtain accurate results, such simulations or emulations must include an adequate model of the *Internet delay space*: The all-pairs set of static round-trip propagation delays among edge networks. Such a model must accurately reflect those characteristics of real Internet delays that influence system performance. For example, having realistic clustering properties is important because they can influence the load balance of delay-optimized overlay networks, and the effectiveness of server placement policies and caching strategies. Having realistic growth characteristics [16] in the delay space is equally important, because the effectiveness of certain distributed algorithms depends on them. Many distributed systems are also sensitive to the inefficiency of IP routing with respect to delay. Such inefficiency manifests itself as triangle inequality violations in the delay space, and must be reflected in a model as well.

Currently, two approaches are used to obtain a delay model. The first approach, adopted for instance by the P2PSim simulator [25], is to collect actual delay measurements using a tool such as King [13]. However, due to limitations of the measurement methodology and the quadratic time requirement for measuring a delay matrix, measured data tends to be incomplete and there are limits to the size of a delay matrix that can be measured in practice. To its credit, P2PSim provides a $1740\times1740$ delay space matrix, which is not a trivial amount of data to obtain.

The second approach is to start with a statistical network topology model (e.g. [45, 48, 8, 10, 18]) and assign artificial link delays to the topology. The delay space is then modeled by the all-pair shortest-path delays within the topology. The properties of such delay models, however, tend to differ dramatically from the actual Internet delay space. This is because these models do not adequately capture rich features in the Internet delay space, such as those caused by geographic constraints, variation in node concentrations, and routing inefficiency.

A delay space model suitable for large-scale simulations must adequately capture the relevant characteristics of the Internet delay space. At the same time, the model must have a compact representation, since large-scale simulations tend to be memory-bound. The naive approach of storing 16-bit delay values for all pairs of a 100K node network, for instance, would require almost 20GB of main memory! Finally, to enable efficient simulation, generating a delay value for a given pair of nodes must require very little computation and no disk accesses.

One approach is to build a *structural* model of the Internet, using BGP tables, traceroute, ping and other measurements to capture the coarse-grained (e.g., AS-level) topology of the Internet and the associated static link delays [22]. Given such a model, the delay for a given pair of IP addresses can be estimated by adding the link delays on the predicted route through the topology. If the topology model captures the coarse-grained structure of the Internet well enough, the resulting delays should preserve the characteristics of the Internet delay space. However, it remains unclear how detailed such a model has to be to preserve the relevant characteristics.

Another approach is to build a *statistical* model, designed to preserve the statistical characteristics of a measured Internet delay data set. Unlike a structural model, a statistical model cannot predict the delay between a particular pair of real Internet IP addresses. For the purposes of distributed systems simulations, however, it suffices that the statistical properties of the model adequately reflect those of the measured delay data. Statistical models lend themselves to a compact representation and can enable efficient generation of delay data at large scale. Since we are primarily interested in enabling accurate, efficient, large-scale simulations, we decided to pursue this approach in this paper.

We have measured a sample of the Internet delay space among 3,997 edge networks. We then characterize the measured sample with respect to a set of metrics that are relevant to distributed system design. Based on these analytical findings, we develop a method to model measured Internet delay spaces. The resulting model has a compact $O(N)$ representation (as opposed to the $O(N^2)$ matrix representation) that adequately preserves the relevant delay space characteristics, and can model missing measurements. We then extend our model and develop a method to synthesize an artificial delay space. The method exploits the scaling characteristics found in the measurements and makes it possible to synthesize a delay space much larger than the measured delay space, while preserving the characteristics of the measured data. We make two primary contributions in this work:

- We systematically quantify the properties of the Internet delay space with respect to a set of statistical, structural, and routing metrics relevant to distributed systems design. This leads to new fundamental insights into Internet delay space characteristics that may inform future work.
- We develop a set of building block techniques to model and synthesize the Internet delay space compactly, while accurately preserving the relevant metrics. The compact representation enables accurate and memory efficient network simulations at large scale.

We emphasize that our goal is to provide a model of the Internet delay space that enables accurate large-scale simulations. We do not attempt to provide either an *explanatory* model of Internet delay, which explains the underlying technical, economic and social forces that shape Internet delays, nor do we attempt to provide a *predictive* model that can estimate the delay between a given pair of real IP hosts. Building such models is also an interesting research direction, but is beyond the scope of this paper.

## 2. METHODOLOGY AND MODELS

We begin by describing our measurement methodology and the existing delay space models we use in this study.

### 2.1 Measured Internet Delay Space

We use the King tool [13] to measure the all-pair round-trip static propagation delays among a large number of globally distributed DNS servers, where each server represents a unique domain and typically one edge network. To choose DNS servers, we start with a list of 100,000 random IP addresses drawn from the prefixes announced in BGP as published by the Route Views project [32]. For each IP address, we perform a reverse DNS lookup to determine the associated DNS servers. Each reverse lookup returns a set of DNS servers $D_{IP_i}$. We keep only the DNS server sets in which at least one server supports recursive queries, since King requires it. If two DNS server sets $D_{IP_i}$ and $D_{IP_j}$ overlap, then only one of the two sets is kept since they do not represent distinct domains. If there is more than one server in a set, the set is kept only if all the servers in the set are topologically close. We check this by performing traceroutes to all the servers in the set. By making sure the servers in the set are physically co-located, we ensure different measurement samples are measuring the same network. Among the remaining DNS server sets, we choose one server per set that supports recursive query. We then use 5,000 such DNS servers to conduct our measurements.

Care must be taken during the measurement process. The measured delays include the DNS server processing delays as well as network queuing delays. We collect multiple measurement samples and keep only the minimum value to approximate the static delay. However, high packet loss rates can cause insufficient measurement samples. Also, because King measures the delay between two servers, say $D_1$ and $D_2$, by subtracting the delay to $D_1$ from the delay to $D_2$ *via* $D_1$, it is possible to end up with a very small or even negative delay value if the measurements were tainted by processing or queuing delays.

To ensure the subsequent analysis is based on accurate data, we adopt a fairly stringent methodology. We measure the round-trip delay between two DNS servers from both directions by using either server as the recursive server. For each direction, we make up to 50 attempts to measure the recursive delay to $D_2$ via $D_1$, and up to 50 attempts to measure the delay to $D_1$ via $D_2$. At least 20 measurement samples must be obtained in each case. The minimum value across the samples is used as the propagation delay. After the subtraction step, if the delay is negative, or if the delay is greater than 2 seconds or smaller than 100 microseconds, it is discarded. These unrealistic delay values are likely caused by processing and queuing delays that affected the measurements. Also, if the obtained delay between $D_1$ and $D_2$ measured in each direction disagrees by more than 10%, we discard the measurement. Finally, we remove data from DNS servers that are consistently failing to provide valid measurements: After we assemble the delay space matrix, if any row/column has more than 25% of the values missing, the entire row/column is removed.

We collected the measurements in October 2005. Among the collected 5000$\times$5000 delay data, 16.7% have insufficient measurements samples, 8.1% have inconsistent samples, 0.16% are smaller than 100 microseconds, and 0.51% are larger than 2 seconds. After removing suspicious measurement values, the remaining delay matrix has 3997 rows/columns with 13% of the values in the matrix unavailable. To characterize the distribution of the missing values, we partition the delay matrix into its three largest clusters. These clusters correspond to IP hosts in North America, Europe and Asia. We find that the percentage of missing values are distributed as follows:

| From/To | North America | Europe | Asia |
|---|---|---|---|
| North America | 14% | 11% | 12% |
| Europe | 11% | 15% | 11% |
| Asia | 12% | 11% | 18% |

To understand the properties in the data set under scaling, we consider four different random sub-samples of the measured data with the sizes 800, 1600, 2400, and 3200. To reduce the sensitivity to a particular random sample, for each sub-sample size, we consider five random sample. Results presented in this paper are averages over the five samples.

## 2.2 Topology Model Delay Spaces

We also generate delay matrices based on existing topology models and compare them against the measured Internet delay space. The two generators we use are Inet [46] and GT-ITM [48]. The Inet generator creates a topology that has power-law node degree distribution properties. The GT-ITM generator is used to generate a topology based on the Transit-Stub model. We include the Inet and GT-ITM topology models in this study because they are often used in distributed system simulations.

For Inet, we create a 16000-node topology. To generate the delays, we use the standard method of placing nodes randomly in a plane and then use the Euclidean distance between a pair of connected nodes as the link delay. All-pairs shortest delay routing is then used to compute end-to-end delays. Finally, we extract the generated delays among the 5081 degree-1 nodes in the graph in order to model the delays among edge networks. No triangle inequality violations are introduced. For GT-ITM, we create a 4160-node transit-stub topology. Note that GT-ITM annotates links with routing policy weights and artificial delays. Shortest path routing is performed over the topology using routing policy weights as the link costs. End-to-end delays are then computed by summing the artificial link delays along the selected paths. Some triangle inequality violations are then introduced artificially in the resulting delay space. Finally, we extract the delays among 4096 stub routers to model the delays among edge networks.

We scale the delays in the two artificial delay matrices such that their average delay matches the average delay in the measured delay data. This constant scaling does not affect the structure of the generated delay spaces. We do this only to simplify the presentation of results.

## 2.3 Limitations of Measured Delay Data

Our analysis is based on a carefully collected set of measured Internet delay data. The data set, however, does have limitations. First, the measurements are among DNS servers. The data set thus represents the delay space among edge networks in the Internet. No explicit measurements were collected among hosts *within* a local area network. For example, even though a university campus may have thousands of hosts, we most likely pick only one of its DNS servers to include in the measurement. Therefore, this study addresses only the delay space properties among edge networks in the wide area, but not the delay space properties within a local area network. Secondly, to increase our confidence in the data, we have discarded questionable measurements. We therefore proceed with the assumption that the missing delay values do not have significantly different properties than the available data.

## 3. INTERNET DELAY SPACE ANALYSIS

In this section, we first identify a set of metrics that are known to significantly influence the performance of distributed systems. Then, we analyze measured Internet delay data with respect to these and other statistical and structural properties. The results give insight into the characteristics of the Internet delay space, and they inform the design of an appropriate model.

## 3.1 Systems-motivated Metrics

The metrics presented below are known to strongly influence distributed system performance and capture a wide range of important issues in distributed system design and evaluation.

**Global clustering** - This metric characterizes clustering in the delay space at a macroscopic level. For instance, the continents with the largest concentration of IP subnetworks (North America, Europe and Asia) form recognizable clusters in the delay space. This global clustering structure is, for instance, relevant to the placement of large data centers and web request redirection algorithms (e.g. [29]).

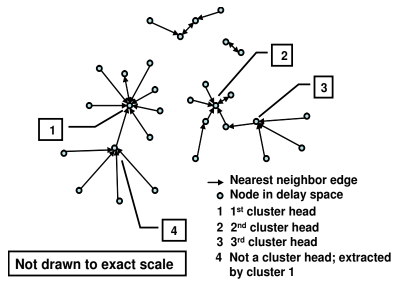

**Figure 1: Nearest neighbor directed graph analysis technique.**

Our algorithm to determine the global clustering works as follows. Given N nodes in the measured input data, it first treats each node as a singleton cluster. The algorithm then iteratively finds two closest clusters to merge. The distance between two clusters is defined as the average distance between the nodes in the two clusters. A cutoff delay value determines when to stop the merging process. If the distance between the two closest clusters is larger than the cutoff, the merging process stops. By varying the cutoff value and monitoring the resulting cluster sizes, the global clustering properties can be determined.

**Local clustering** - This metric characterizes clustering in the delay space at the local level. It is based on analyzing the in-degree distribution of the directed graph formed by having each node point to its nearest neighbor in the delay space. Moreover, we use the graph to identify a set of local cluster heads (or centers). We select the node with the highest in-degree as a local cluster head and remove it and its immediate children from the graph. This step is applied repeatedly to identify the next local cluster head until no more nodes remain. Since a local cluster resembles a star graph, we sometimes simply call it a star. The process is illustrated in Figure 1. The importance of the local cluster heads will become clear in subsequent sections.

Local clustering is relevant, for instance, to the in-degree and thus the load balance among nodes in delay-optimized overlay networks (e.g. [5]). For example, dense local clustering can lead to an overlay node having an unexpectedly high number of neighbors and can potentially create a load imbalance in the overlay.

**Growth metrics** - Distributed nearest neighbor selection is a hard problem, but efficient algorithms have been identified to solve the problem for growth-restricted metric spaces [16]. These algorithms are used, for instance, in Tapestry [49] and Chord [41] to select overlay neighbors. In a growth-restricted metric space, if the number of nodes with a delay of at most $r$ from some node $i$ is $B_i(r)$, then $B_i(2r) \leq c \cdot B_i(r)$, where $c$ is a constant. We characterize the growth properties of a delay space by evaluating the function $B(2r)/B(r)$.

A related metric is the $D(k)$ metric. Let $d(i,k)$ be the average delay from a node $i$ to its $k$ closest nodes in the delay space and $N$ be the set of nodes, then $D(k) = \frac{1}{|N|}\sum_{i \in N} d(i,k)$. Structured overlay networks like Chord, Tapestry and Pastry employ proximity neighbor selection (PNS) to reduce the expected delay stretch $S$, i.e., the ratio of the delay of an overlay route over the direct routing delay averaged over all pairs of nodes [14, 4, 30, 5]. We choose to include the $D(k)$ metric because analysis has shown that in Tapestry and Pastry, the expected delay stretch $S$ in the overlay can be predicted based on the function $D(k)$ [5].

**Triangle inequality violations** - The triangle inequality states that given points $x$, $y$ and $z$ in a Euclidean space, the distance $d_{ij}$ between points $i$ and $j$ satisfies $d_{xz} \leq d_{xy} + d_{yz}$. The Internet delay space, however, does not obey the triangle inequality, since Internet routing may not be optimal with respect to delay. Unfortunately, many distributed nearest neighbor selection algorithms rely on the assumption that the triangle inequality holds [33, 16, 44]. Thus, it is important to characterize the frequency and severity of the violations in the Internet delay space.

| Sample size | # Cluster heads | Percentage |
|---|---|---|
| 800 | 185 | 23.1% |
| 1600 | 363 | 22.7% |
| 2400 | 547 | 22.8% |
| 3200 | 712 | 22.3% |
| 3997 (all data) | 884 | 22.1% |

**Table 1: Average fraction of nodes classified as cluster heads in measured data.**

## 3.2 Analysis Results

We now present an analysis of the measured delay data with respect to the metrics described above, and some basic properties like the delay distribution. For comparison, we also show the relevant properties of the delays produced by the Inet and GT-ITM models.

We begin with a comparison of the delay distribution. In Figure 2(a), we can observe that the delay distributions of the measured data set have characteristic peaks at roughly 45ms, 135ms, and 295ms. This suggests that the nodes form clusters in the data. Analysis of random data sub-samples indicates that the delay distribution is also independent of sample size. In contrast, the delay distributions for the topology models do not indicate such behavior. Clearly, there are rich features in the Internet delay space that are not captured in the delays derived from these topology models.

To visualize the locations of nodes, we first embed the data sets into a 5D Euclidean space using a dimensionality reduction procedure that is robust to missing data. Then, we do a principal component analysis on the 5D Euclidean coordinates to get the first 2 principal components. Several techniques exist to compute the 5D embedding [24, 7, 35, 6, 19, 43]. Here, we use a slightly modified version of the Vivaldi [7] method that avoids the missing measurements. We use 32 neighbors per node in Vivaldi.

Figure 2(b) displays the scatter plots of the first two principal components of the 5D embedding for different data sets. The visual differences between the measured data and the topology models are striking. It is easy to see that there exists clustering structure in the measured data. In contrast, the nodes in the topology models are distributed more uniformly in the space, and their resulting delay distributions are approximately normal.

To quantify the global clustering properties in the measured data set, we apply the described global clustering algorithm and plot the percentage of nodes in the largest cluster against different clustering cut-off thresholds in Figure 2(c). Regardless of the sample size, the largest cluster's size increases sharply at cutoff values 155ms and 250ms. These sharp increases are caused by the merging of two clusters at these thresholds. The steps suggest that there are three dominant clusters. By setting the threshold to 120ms, nodes can be effectively classified into the three major clusters. They account for 45% (the North America cluster), 35% (the Europe cluster), and 9% (the Asia cluster) of the nodes, respectively. The remaining 11% are nodes that are scattered outside of the major clusters. These global clustering properties can be used to guide the global placement of servers and the design of load-balancing algorithms. In contrast, there is no clear clustering structure in the Inet model. The clustering structure of the GT-ITM model also does not resemble that of the measured data.

The global clustering analysis reveals the coarse-grained structure of the delay space. To understand the fine-grained structure, we conduct the nearest neighbor directed graph analysis on the data sets. We emphasize that these results characterize the properties among edge networks in the Internet; they *do not* characterize the properties among end hosts within local area networks. Figure 3(a) shows the in-degree distributions for different sample sizes. Observe that the in-degree distribution for the measured data has an exponential decay (note the log-linear scale). Interestingly, we discover that the distribution is consistent across different sample sizes. If a straight line is fitted over 99.9% of the distribution (i.e., ignoring the 0.1% of nodes with the largest in-degrees), the line has a y-intercept of -0.8565 and a slope of -0.6393. These parameters can be used to model the nearest-neighbor in-degree distribution among edge networks in the Internet. In the future, when delay data for hosts within local area networks become available, the model can be hierarchically extended by assigning end hosts appropriately to each edge network in the model.

We classify the nodes into local cluster heads (or star heads) and non-heads using the procedure described in 3.1. Table 1 shows that the proportion of nodes in the data that are classified as local cluster heads is quite stable across different sample sizes. This observation is also true when each major global cluster is considered separately. This property will be useful when we turn to the synthesis of delay spaces later in this paper.

In contrast, as shown in Figure 3(b), the in-degree distribution for the Inet topology follows closely the power-law (note the log-log scale). If a straight line is fitted over 99.9% of the distribution, the line has a y-intercept of -3.7852 and a slope of -1.3970. Thus, the Inet model does not reflect the local clustering properties among edge networks in the measured delay data. For the GT-ITM topology, as shown in Figure 3(c), the distribution is close to exponential, the best fit line in the log-linear plot has y-intercept of -0.0080 and slope of -1.1611. Thus, this distribution is also different from that found in the measured data.

Next we analyze spatial growth. Figure 4(a) shows the median $B(2r)/B(r)$ growth of the data sets. We plot the median because, unlike the mean, it is insensitive to the extreme outliers and can better characterize the dominant trends. As can be seen, the topology models have far higher peak spatial growth than the measured data (note the log-linear scale) and have very different trends. In the measured data, the initial growth is higher when the ball is expanding within a major cluster. As soon as the ball radius covers most of the nodes within the same major cluster, growth slows down as expected. When the ball radius reaches a size that begins to cover another major cluster, the growth increases again. Eventually most of the nodes are covered by the ball and the growth ratio steadily drops to one. This growth trend in the measured data is invariant across different sample sizes. These new findings can help fine tune distributed system algorithms that are sensitive to the ball growth rate. On the other hand, the growth trends in the Inet and GT-ITM topology models do not reflect the structure of the measured data.

In terms of the $D(k)$ metric, we also observe dramatic differences between topology models and the measured data. Figure 4(b) indicates that in the Inet and GT-ITM topology models, from the perspective of an observer node, there are very few nodes whose delays are substantially smaller than the overall average delay. In contrast, in the measured data, from an observer node, we can find many more nodes whose delays are substantially smaller than the

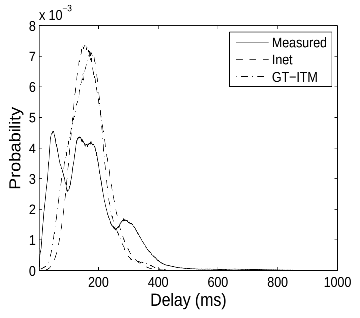

(a)

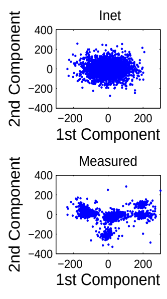

(b)

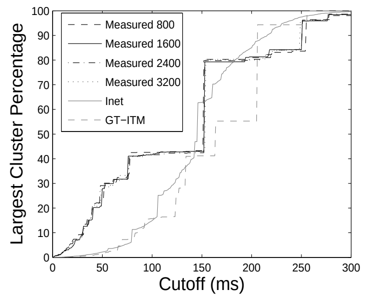

(c)

**Figure 2: Global clustering properties. (a) Delay distribution. (b) 2D coordinates scatter plot. (c) Clustering results.**

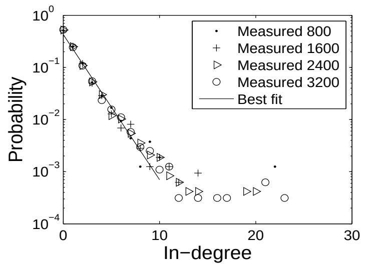

(a)

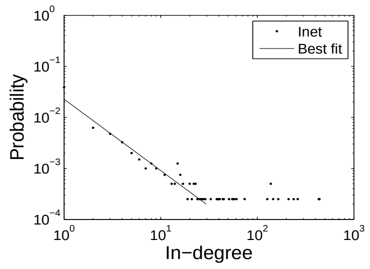

(b)

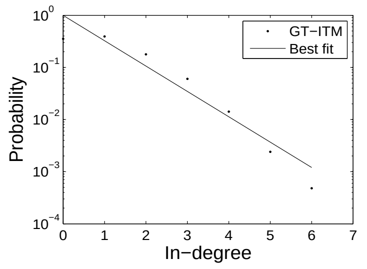

(c)

**Figure 3: Local clustering analysis. (a) Exponential-like in-degree distribution for measured data (log-linear scale). (b) Power-law-like in-degree distribution for Inet (log-log scale). (c) Exponential-like in-degree distribution for GT-ITM (log-linear scale).**

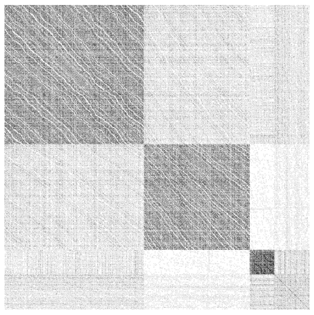

**Figure 5: Type 1 triangle inequality violations for Measured Data (white color is most severe).**

overall average. Thus, a random probing strategy for finding a close-by neighbor would be much more successful in the real Internet than in the Inet and GT-ITM topology models. This is an example of how using an inadequate delay space model for simulation can potentially lead to misleading results. Finally, it can be observed that the $D(k)$ metric is also invariant across different sample sizes. This empirical $D(k)$ function can be applied to compute the expected delay stretch in the Pastry and Tapestry overlays when deployed over the global Internet [5].

We next analyze the measured data set with respect to properties related to triangle inequality violations. We say that an edge $ij$ in the data set causes a Type 1 triangle inequality violation if for some node $k$, $\frac{d_{ik}+d_{kj}}{d_{ij}} < 1$, and it causes a Type 2 violation if $\frac{|d_{ik}-d_{kj}|}{d_{ij}} > 1$. Intuitively, better overlay paths can be found for edges that cause Type 1 violations, and edges that cause Type 2 violations can potentially provide short-cut overlay paths.

For each edge $ij$, we count the number of Type 1 violations it causes. To illustrate how the number of triangle inequality violations are distributed over the major clusters, we present a matrix in Figure 5 for the measured data. To produce this figure, we first reorganize the original data matrix by grouping nodes in the same clusters together. The top left corner has indices (0,0). The matrix indices of the nodes in the largest cluster (North America) are the smallest, the indices for nodes in the second largest cluster (Europe) are next, then the indices for nodes in the third largest cluster (Asia), followed by indices for nodes that did not get classified into any of the 3 major clusters.

Each point $(i, j)$ in the plot represents the number of Type 1 violations that the edge $ij$ is involved in as a shade of gray. A black point indicates no violation and a white point indicates the maximum number of violations encountered for any edge in the analysis. Missing values in the matrix are drawn as white points.

It is immediately apparent that clustering is very useful for classifying triangle inequality violations. It can be seen that edges within the same cluster (i.e. the 3 blocks along the diagonal) tend to have significantly fewer Type 1 violations (darker) than edges that cross clusters (lighter). Also, the number of violations for edges connecting a given pair of clusters is quite homogeneous. Note that the white wavy lines roughly parallel to the diagonal are simply showing the missing data. Our measurement methodology measures the data in sequences parallel to the diagonal to evenly spread the traffic among the probed DNS servers. Thus, when a measurement station fails, an entire diagonal can be missing. The lines are not straight because whole rows and columns are removed from the data set if they have more than 25% of the values missing. Due to space limitations, we do not include the matrix picture for Type 2 violations, but as expected, the relative shades are the reverse of those in Figure 5. These results imply that, if two nodes are within

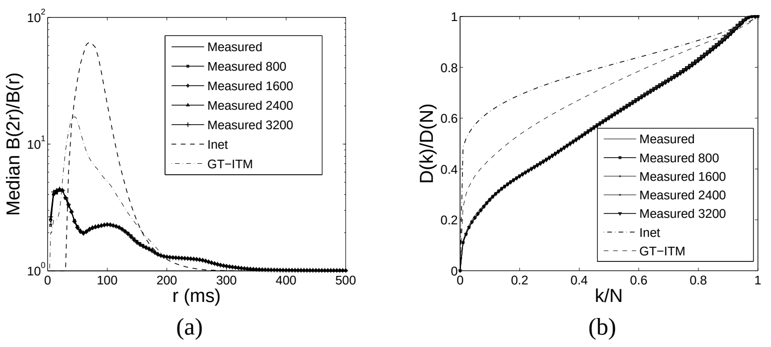

**Figure 4: Growth metrics. (a)** $B(2r)/B(r)$ **metric (log-linear scale). (b)** $D(k)/D(N)$ **metric.**

the same major cluster, then the chance of finding a shorter overlay path is far lower then when the nodes are in different clusters. Moreover, edges that are used to form better overlay paths are most likely found inside a cluster. Interestingly, observe that it is least likely to find better overlay routes for paths within the Asia cluster, but it is easiest to find better overlay routes for paths across the Asia and Europe clusters.

We show in Figure 6(a) and Figure 6(b) the cumulative distributions of Type 1 and Type 2 violation ratios for different sample sizes. Observe that the distribution is very stable across sample sizes. Intuitively, since triangle inequality violation is an inherent property of the inefficiency of Internet routing, the amount of triangle inequality violations observed is not expected to depend on the number of data samples. This invariant is useful in synthesizing the Internet delay space.

## 3.3 Summary

Our analysis confirms some existing knowledge about the Internet delay space, such as the characteristic delay distribution and continental clustering. In addition, the analysis provides a number of new insights:

• The in-degree distribution of the directed nearest neighbor graph of the measured data resembles an exponential distribution and is stable across sample sizes. The relative number of local clusters also appears stable across sample sizes. These findings can be used to model local clustering properties in the Internet delay space.

• The ball growth metrics reflect the continental clustering structure of the delay space and the observed growth rate is low. These properties can inform the design of distributed algorithms, for instance to find the nearest neighbor. The $D(k)$ function empirically derived from the data shows that it is not difficult to encounter a close-by neighbor by random probing. The function can also be used to compute the expected delay stretch in structured overlay networks.

• The potential benefit of overlay routing for a pair of nodes $ij$ and the utility of the pair for overlay routing can be predicted by the clusters that $i$ and $j$ belong to. In particular, it is hardest to find better overlay routes for paths within the Asia cluster, but it is easiest to find better overlay routes for paths across the Asia and Europe clusters.

• Delay spaces derived from existing Internet topology models are dramatically different from the Internet delay space. Understanding these differences can help practitioners to design better evaluation methodologies, more correctly interpret their results, and avoid drawing incorrect conclusions.

## 4. INTERNET DELAY SPACE MODELING

Using measured Internet delay data to drive distributed system simulations allows system designers to evaluate their solutions under realistic conditions. However, there are two potential concerns. First of all, our ability to measure a large portion of the Internet delay space is limited by the time required and the difficulty of dealing with network outages, measurement errors and accidentally triggered intrusion alerts. The second concern is that the $O(N^2)$ storage requirement of a measured delay matrix representation does not scale.

To address these concerns, we develop techniques to model a measured Internet delay space. This model adequately preserves the relevant properties of the measured data, and it has only $O(N)$ storage overhead. Later in this paper, we will also present techniques to synthesize realistic delay data for a much larger delay space than can be measured in practice so as to enable realistic large-scale simulations.

## 4.1 Building Block Techniques

**Technique 1: Low-dimensional Euclidean embedding** - The first technique we use is to model an Internet delay space using a low-dimensional Euclidean embedding. That is, we compute Euclidean coordinates for each node and use Euclidean distances to model the delays in the delay space. Such a Euclidean map has a scalable $O(N)$ representation.

Although several techniques exist to compute a Euclidean embedding robustly [24, 7, 35, 6, 19, 43, 40, 39], and previous studies have shown that an Internet delay space can be overall well approximated by a Euclidean embedding with as little as 5 dimensions, such an embedding tends to inflate the small values ($<$ 10ms) in the delay space too much [17].

In order to create a model that also preserves small values, we first use the Vivaldi algorithm to create a 5D Euclidean embedding of the measured delay space, then we explicitly adjust the Euclidean coordinates of nodes as follows. First, extract the set $S$ of all node pairs $(i, j)$ with measured delay $d_{ij}$ less than 10ms. Next, among these node pairs, select the node pair $(m, n)$ whose Euclidean distance $\hat{d}_{mn}$ in the embedding is smallest. If $\hat{d}_{mn} > 30ms$, the procedure terminates. Otherwise, the coordinates of node $m$ and $n$ are adjusted so that $\hat{d}_{mn}$ becomes identical to $d_{mn}$. Then, $(m, n)$ is removed from $S$ and the procedure repeats. The effect of this procedure is that small values in the measured delay space that are mildly distorted in the initial Vivaldi 5D Euclidean embedding are well preserved by the final set of adjusted Euclidean coordinates. These adjusted Euclidean coordinates serve as the starting point for our model.

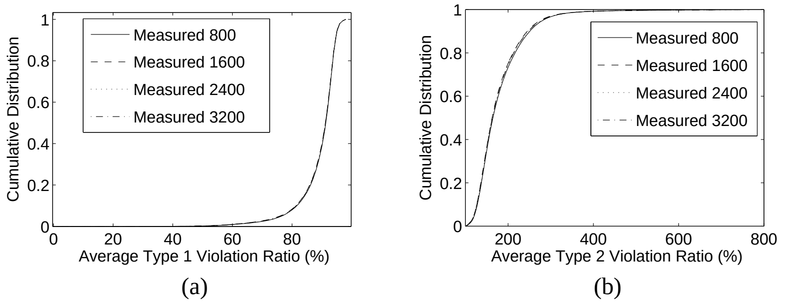

**Figure 6: Triangle inequality violation ratio distributions. (a) Type 1 violations. (b) Type 2 violations.**

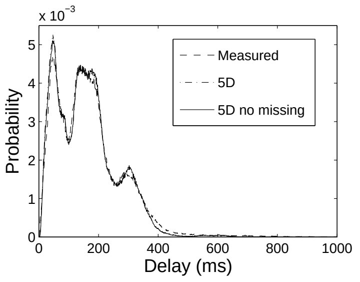

**Figure 7: Delay distribution of the 5D Euclidean map.**

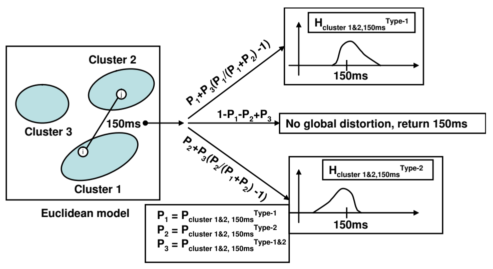
Cluster 2
Cluster 3
Cluster 1
j
i
150ms
Euclidean model
P1+P3(P1/(P1+P2) -1)
1-P1-P2+P3
P2+P3(P2/(P1+P2) -1)
H cluster 1&2,150ms Type-1
150ms
No global distortion, return 150ms
H cluster 1&2,150ms Type-2
150ms
P1 = P cluster 1&2, 150ms Type-1
P2 = P cluster 1&2, 150ms Type-2
P3 = P cluster 1&2, 150ms Type-1&2

**Figure 8: Global distortion technique.**

Figure 7 shows the delay distributions for (1) the measured data, (2) all the delays in the 5D Euclidean map, including the modeled values for the missing data, and (3) the delays in the 5D Euclidean map corresponding to the available measured data. We can see that the 5D Euclidean map preserves the distribution of the measured delay values well. In addition, the modeled values for the missing data do not skew the overall distribution.

However, a Euclidean embedding cannot preserve triangle inequality violations. The Euclidean map also fails to preserve the high in-degree of some nodes in the nearest neighbor directed graph. This is because a node cannot have a high number of nearest neighbors in a low-dimensional Euclidean space. Specifically, the maximal in-degree is 12 in the measured delay space, and only 5 in the 5D map. To address these limitations of the basic 5D Euclidean model, we use two additional techniques in order to preserve the properties lost as a result of the Euclidean embedding.

**Technique 2: Global distortion** - The basic technique to create triangle inequality violations in the 5D Euclidean model is to distort the delays computed from the 5D embedding. Since the frequency of triangle inequality violations in the measured data is relatively small, it suffices to distort only a small subset of node pairs or edges.

The idea is to take into consideration that edges between different pairs of global clusters have very different triangle inequality violation behavior (as can be seen in Figure 5), identify the edges in each pair of clusters that cause violations above a certain severity threshold, characterize the distortion distribution for these edges when they are mapped into the 5D Euclidean model, then use this same distortion distribution to introduce distortions when delays are generated from the 5D embedding. To ensure that the model always produces the same delay for a given pair of nodes, it uses the node identifiers to generate deterministic pseudo-random distortions. By choosing different severity thresholds, we can vary the number of edges that get distorted in the model and experimentally determine the threshold that best matches the empirical data. An overview of the technique is illustrated in Figure 8.

We define a violation severity threshold $R$. A violation caused by an edge $ij$ is severe if for some node $k$, $\frac{d_{ik}+d_{kj}}{d_{ij}} < R$ (called Type 1 violation), or if $\frac{|d_{ik}-d_{kj}|}{d_{ij}} > \frac{1}{R}$ (called Type 2 violation). For each global cluster pair $g$, all edges with the same 5D Euclidean model delay $l$ (rounded down to the nearest 1ms) form a subgroup. For each subgroup $(g,l)$, we compute the fraction of edges in this subgroup that are involved in severe Type 1 violations in the measured data, $P_{g,l}^{Type-1}$, and a histogram $H_{g,l}^{Type-1}$ to characterize the real delay distribution of those severe violation edges. Similarly, for Type 2 violations, we compute the fraction $P_{g,l}^{Type-2}$ and the histogram $H_{g,l}^{Type-2}$. We also compute the fraction of edges that incur severe Type 1 and Type 2 violations simultaneously, $P_{g,l}^{Type-1\&2}$. This extra statistical information incurs an additional constant storage overhead for the model.

With these statistics, the delay between node $i$ and $j$ is then computed from the model as follows. Draw a pseudo-random number $\rho$ in [0,1] based on the IDs of $i$ and $j$. Let the Euclidean distance between $i$ and $j$ be $l_{ij}$ and the cluster-cluster group be $g$. Based on $P_{g,l_{ij}}^{Type-1}$, $P_{g,l_{ij}}^{Type-2}$, $P_{g,l_{ij}}^{Type-1\&2}$, and using $\rho$ as a random variable, decide whether the edge $ij$ should be treated as a severe Type 1 violation (with probability $P_{g,l_{ij}}^{Type-1} + P_{g,l_{ij}}^{Type-1\&2} \cdot (\frac{P_{g,l_{ij}}^{Type-1}}{P_{g,l_{ij}}^{Type-1}+P_{g,l_{ij}}^{Type-2}} - 1)$), or a severe Type 2 violation (with probability $P_{g,l_{ij}}^{Type-2} + P_{g,l_{ij}}^{Type-1\&2} \cdot (\frac{P_{g,l_{ij}}^{Type-2}}{P_{g,l_{ij}}^{Type-1}+P_{g,l_{ij}}^{Type-2}} - 1)$), or to return the value $l_{ij}$ without distortion. If the edge $ij$ is treated as a severe Type 1 violation, then we use the histogram $H_{g,l_{ij}}^{Type-1}$ and $\rho$ to draw a value from the histogram and return that value. Similarly, if the edge is treated as a severe Type 2 violation, then we use the histogram $H_{g,D_{ij}}^{Type-2}$ instead.

By experimenting with different threshold values $R$, we have determined that a value of 0.85 produces Type 1 and Type 2 violation

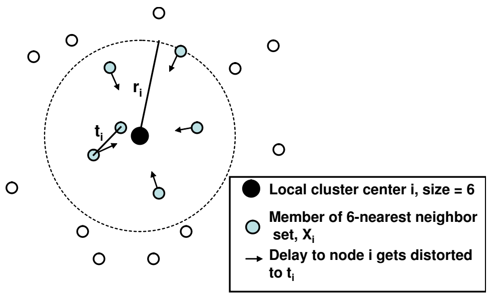
$r_i$
$t_i$
Local cluster center i, size = 6
Member of 6-nearest neighbor set, $X_i$
Delay to node i gets distorted to $t_i$

**Figure 9: Local distortion technique.**

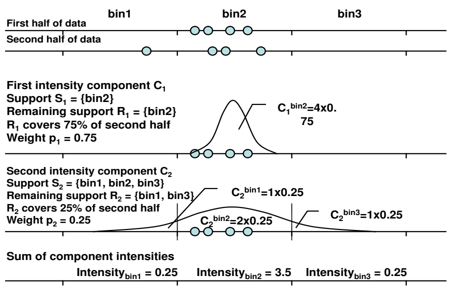
bin1
bin2
bin3
First half of data
Second half of data
First intensity component $C_1$
Support $S_1$ = {bin2}
Remaining support $R_1$ = {bin2}
$R_1$ covers 75% of second half
Weight $p_1$ = 0.75
$C_1^{bin2}$=4x0.75
Second intensity component $C_2$
Support $S_2$ = {bin1, bin2, bin3}
Remaining support $R_2$ = {bin1, bin3}
$R_2$ covers 25% of second half
Weight $p_2$ = 0.25
$C_2^{bin1}$=1x0.25
$C_2^{bin2}$=2x0.25
$C_2^{bin3}$=1x0.25
Sum of component intensities
$\text{Intensity}_{bin1}$ = 0.25
$\text{Intensity}_{bin2}$ = 3.5
$\text{Intensity}_{bin3}$ = 0.25

**Figure 11: Computing intensities in Euclidean map synthesis technique.**

distributions similar to those observed in the measured data. This is also the threshold we use in the remainder of this paper.

**Technique 3: Local distortion** - To preserve the local clustering properties, we introduce additional local distortion. The idea is to simply pull some nodes within a radius around a local cluster center closer to create the needed in-degree, as illustrated in Figure 9. From the nearest neighbor directed graph analysis on the measured data, we identify local cluster centers and note their sizes. Suppose a local cluster center node $i$ has a cluster size of $s_i$ in the original data. We identify the set of its $s_i$ nearest neighbors, $X_i$, in the model after global distortion. Then, we compute a radius $r_i$ as $\max_{j \in X_i}(d_{ij})$, and a threshold $t_i$ as $\min_{j,k \in X_i}(d_{jk}) - \epsilon$. Currently, $\epsilon$ is set to $0.01 \cdot \min_{j,k \in X_i}(d_{jk})$. Then we associate the values $r_i$ and $t_i$ with node $i$ in the model. $r_i$ is essentially the radius within which distortion may be necessary. $t_i$ is the delay needed to beat the smallest delay among the nodes in $X_i$. This additional information adds a constant storage overhead.

The delay between node $i$ and $j$ is then computed as follows. Suppose the delay for the edge $ij$ after global distortion is $l_{ij}$. If neither $i$ nor $j$ is a local cluster center, $l_{ij}$ is returned. Suppose $i$ is a local cluster center and $j$ is not, then if $l_{ij} \leq r_i$, we return $\min(t_i, l_{ij})$; otherwise, we return $l_{ij}$. The $t_i$ threshold is used to ensure that the nodes in $X_i$ cannot choose one another as their nearest neighbors. After the distortion, they will choose $i$ as their nearest neighbor unless there is a closer node outside of the radius $r_i$. If both $i$ and $j$ are local cluster centers, we pick the one with the smaller node identifier as the center and perform the above steps.

## 4.2 Modeling Framework

Based on the basic techniques described above, the overall framework for modeling a measured Internet delay space is as follows: **Step 1.** Perform global clustering on the measured data to assign nodes to major clusters. Perform nearest neighbor directed graph analysis to identify local cluster centers and their sizes. **Step 2.** Compute a 5D Euclidean embedding of the measured data using a robust method. Then, adjust coordinates to preserve small values. **Step 3.** For each cluster-cluster group $g$ and Euclidean model delay $l$, compute the global distortion statistics $P_{g,l}^{Type-1}$, $P_{g,l}^{Type-2}$, $P_{g,l}^{Type-1\&2}$, $H_{g,l}^{Type-1}$, $H_{g,l}^{Type-2}$ using a severe violation threshold $R$. For each local cluster center $i$, compute the local distortion statistics $r_i$ and $t_i$. **Step 4.** At this point, the original measured data is no longer needed. To compute the model delay between node $i$ and $j$, first compute the Euclidean model delay, then apply global distortion if necessary, and finally apply local distortion if necessary. Return final value. The total storage overhead of the model is $O(N)$ and calculating the delay of an edge at run time is simple and has constant cost.

## 4.3 Evaluating the Model

We evaluate the effectiveness of our modeling framework by comparing the properties found in the measured data against properties in the resulting model. Figure 10 presents our results. Overall, we can see that the model preserves all the characteristics of the delay space that we had identified. As expected, there are some small discrepancies. As we will show in the rest of this paper, these small discrepancies do not negatively impact the ability to synthesize realistic artificial delay spaces.

## 5. INTERNET DELAY SPACE SYNTHESIS

In this section, we build upon our empirical understanding of the Internet delay space and our delay space modeling techniques and investigate additional techniques to enable artificial *synthesis* of a realistic delay space. The goal is to allow synthesis of delay spaces at scales that exceed our capability to measure Internet delays. Such a tool is valuable for distributed system design and evaluation.

## 5.1 Building Block Techniques

The new techniques introduced in this section exploit the scaling properties found in the measured Internet delay space to enable the synthesis of a larger delay space.

**Technique 4: Euclidean map synthesis** - Given a 5D Euclidean map of an Internet delay space, we seek to capture its locality and growth characteristics so that we can synthesize an artificial map based on these characteristics and create realistic structure in the synthesized delay space.

A simple idea is to divide the Euclidean space into equal sized hyper-cubes, count the number of points in each hyper-cube, and use these counts as relative intensities. With appropriate scaling of the relative intensities, one can synthesize an artificial map of a certain size by generating random points in each hyper-cube according to the intensities using an inhomogeneous Poisson point process [20, 31][1]. Indeed, this simple method can mimic the point distribution of the original map and generate a realistic overall delay distribution and global clustering structure. However, this method ignores the growth characteristics in the data. As a result, synthetic points can only appear in hyper-cubes where points were originally found.

To incorporate growth characteristics, the idea is to introduce uncertainties in the locations of each point and compute intensities that predict growth. The idea is best explained with a simple example illustrated in Figure 11. In the example, there are 8 points in

[1]The number of points lying in any two disjoint sets in space are independent random numbers distributed according to a Poisson law with mean given by the intensity.

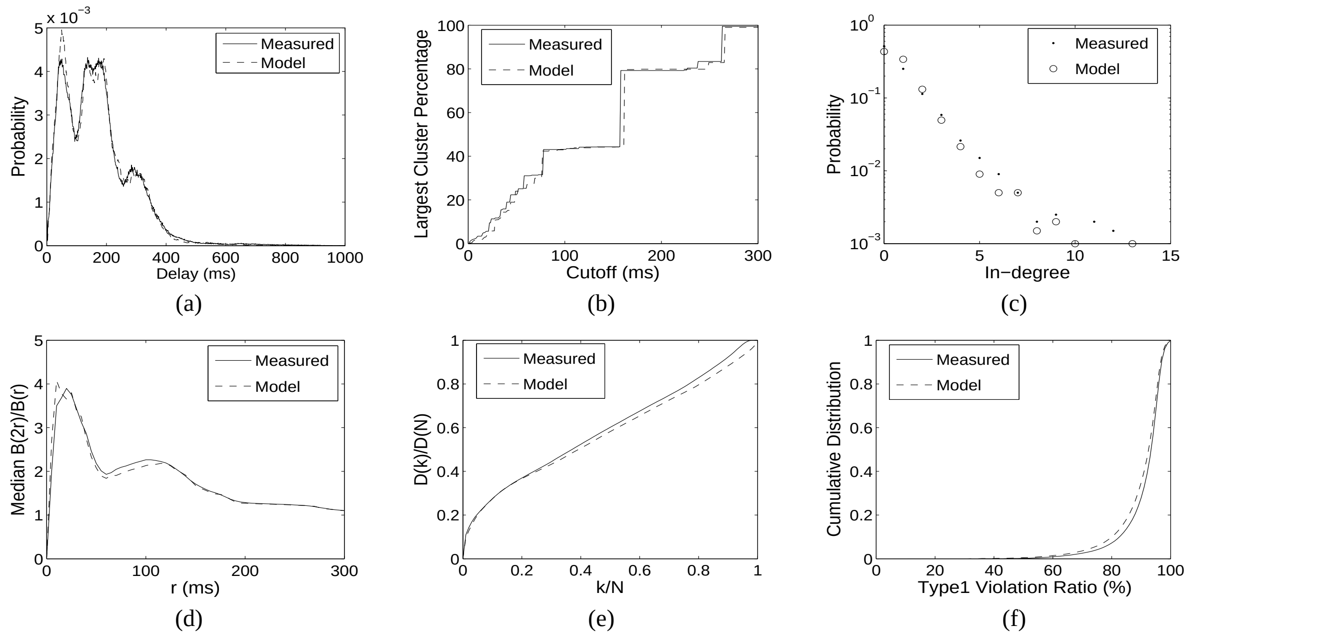

**Figure 10: Model vs measured data. (a) Delay distribution. (b) Clustering cutoff. (c) In-degree distribution. (d) Median B(2r)/B(r). (e) D(k)/D(N). (f) Triangle inequality violation ratio distribution.**

a 1-dimensional Euclidean space divided into 3 equally sized bins. We randomly divide the points into two halves, the first half happens to lie in bin2, while the other half is spread across bin1 and bin2. We will iteratively compute, using the first half of the points, the $i^{th}$ *intensity component* $C_i$, which is a vector of intensities for the bins, to predict the growth observed in the second half of the points. Each component is weighted according to how well it predicts the second half. The location uncertainty of a point in the first half is represented by a Gaussian probability distribution with a certain variance or width. To compute the first intensity component $C_1$, we place a Gaussian with a small *width* $w_1$ that represents a low level of uncertainty in the center of each bin and scale it by the number of first half points in the bin. As a result, the 99% bodies of the Gaussians lie within bin2. We call the bins occupied by the 99% bodies of the Gaussians the *support* of the first component, $S_1$. We also define the *remaining support* of a component to be the support of the current component subtracted by the support of the previous component, i.e. $R_i = S_i \backslash S_{i-1}$. Since this is the first component, $R_1$ is simply $S_1$.

The *intensity* $I_1$ generated by the Gaussians is spread over the three bins as 0, 4, 0, respectively. Now we ask, how well does $R_1$ cover the second half of the points? If all points in the second half are covered by $R_1$ then $I_1$ can account for the growth in the second half and we are done. However, in the example, $R_1$ is only covering 75% of the points in the second half. As a result, we weight the intensity $I_1$ by a factor $p_1 = 0.75$ to obtain the intensity component $C_1$. Since we have not completely accounted for the growth in the second half, we need to increase the location uncertainty and compute the second intensity component $C_2$. To do so, we use a wider Gaussian (width $w_2$) for the second iteration. The aggregate intensity is still 4, but this time, it is spread across all 3 bins. Suppose the intensities generated in the 3 bins are 1, 2, 1, respectively. The 99% body of these wider Gaussians occupy all three bins, thus the support of the second component $S_2$ is the set {bin1, bin2, bin3}. The remaining support $R_2$ is $S_2 \backslash S_1$, i.e. {bin1, bin3}. The fraction of the second half covered by $R_2$ is 25%. Thus, the intensity

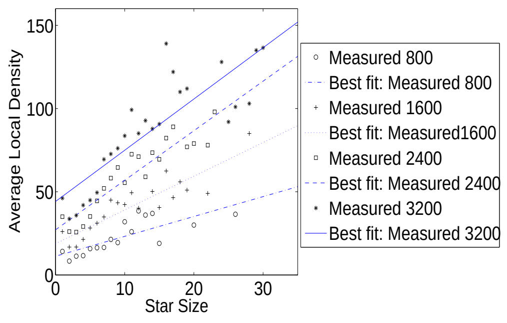

**Figure 12: Average local density vs local cluster (star) size for different data sample sizes.**

$I_2$ is weighted by $p_2 = 0.25$ to obtain $C_2$. This iterative process continues until either all points in the second half are covered by $R_i$, or when a maximum Gaussian width has been reached. The intensity of each bin is simply the sum of all the intensity components $C_i$. Finally, we repeat the procedure to use the second half to predict the growth in the first half and use the average intensity of each bin as the final intensity. In practice, we divide the 5D space into 100 bins in each dimension and vary the Gaussian variance or width from one-tenth to ten times the bin width.

**Technique 5: Local cluster size assignment** - In order to preserve realistic local clustering property, the synthesizer draws the cluster sizes from the exponential distribution (as computed in Section 3.2) that approximates the local cluster size distribution of the measured data. What remains unclear is how to assign different cluster sizes to the synthesized cluster centers. Should the cluster sizes be assigned randomly to the cluster centers? Would that be realistic?

It turns out cluster sizes are related to node densities in the measured data. Figure 12 plots the average local density at the cluster centers, i.e. the number of nodes within 15ms of the cluster centers, versus the local cluster size (or star size) for different sample sizes. As can be seen, the size of a local cluster is roughly linearly related to the local node density around the cluster center.

Therefore, the synthesizer assigns cluster sizes as follows. First, the synthesizer computes the local node densities for the synthesized cluster centers and ranks them according to the densities. The synthesizer also ranks the cluster sizes drawn from the exponential distribution. Then, the synthesizer assigns a cluster center of local density rank $r$ the cluster size of rank $r$. This way, the linear relationship between cluster size and local density is preserved.

## 5.2 Delay Space Synthesizer $DS^2$

Based on the techniques described above and in Section 4.1, we have implemented a delay space synthesizer called $DS^2$ (see [9] for further information). At a high level, $DS^2$ works as follows (Steps 1-3 are identical to those in Section 4.2): **Step 1.** Perform global clustering on the measured data to assign nodes to major clusters. Perform nearest neighbor directed graph analysis to identify local cluster centers. **Step 2.** Compute a 5D Euclidean embedding of the measured data using a robust method. Then, adjust coordinates to preserve small values. **Step 3.** For each cluster-cluster group $g$ and Euclidean delay $l$, compute the global distortion statistics $P_{g,l}^{Type-1}$, $P_{g,l}^{Type-2}$, $P_{g,l}^{Type-1\&2}$, $H_{g,l}^{Type-1}$, $H_{g,l}^{Type-2}$ using a severe violation threshold $R$. **Step 4.** At this point, the original measured data is no longer needed. Split the 5D Euclidean map into two, one containing only local cluster centers, and one containing all other nodes. Then each of the two maps is further divided according to which global cluster each node belongs. Assuming there are three major global clusters and the remaining unclustered nodes form another group, then the splitting procedure produces eight sub-maps. Based on these eight maps, separately synthesize Euclidean maps of each part to the appropriate scale using the Euclidean map synthesis technique. Merge the eight resulting synthesized maps back into one synthesized map. In the final synthesized map, for each node, we now know whether it is a local cluster center and which major cluster it belongs to. **Step 5.** Assign a local cluster size to each synthesized center using the local cluster size assignment technique. For each local cluster center $i$, compute the local distortion statistics $r_i$ and $t_i$. **Step 6.** To compute the synthesized delay between node $i$ and $j$, first compute the Euclidean delay. Apply global distortion, if necessary, according to the statistics from the measured data, and finally apply local distortion if necessary. Return final value.

Note that a lower bound can easily be enforced on the synthesized delays to mimic some sort of minimum processing delay incurred by network devices. $DS^2$ provides this as an option.

## 5.3 Evaluating the Synthesized Delay Model

To evaluate the effectiveness of the synthesized delay model, we first extract a 2,000 node random sub-sample from the measured data. Then, we feed $DS^2$ with just this 2,000 node sub-sample to synthesize delay spaces with 2x, 4x, and 50x scaling factors. If $DS^2$ correctly predicts and preserves the scaling trends, then the synthetic 2x delay space should have properties very similar to those found in the measured data from 3997 nodes. The larger scaling factors (4x and 50x) are presented to illustrate how the synthesizer preserves various properties under scaling. Note that at the scaling factor of 50x, a 100,000 node delay space is synthesized. Unfortunately, at this scale, we do not have efficient ways to compute global clustering (requires $O(N^3)$ space) and triangle inequality violation ratios (requires $O(N^3)$ time) and thus results for these two metrics are calculated based on a 16,000 node random sample out of the 50x synthetic delay space.

The results in Figure 13 show that, even though the synthesis is based on a 2,000 node subset of data, the 2x synthesized data is able to match the characteristics of the 3997 node measured data very well. As expected, there are a few differences. However, these differences are small and we will show in Section 6 that they do not negatively affect the application of the synthesized delay model in distributed system simulations. It is also worth noting that the scaling invariants observed in the measured data are maintained by the synthesizer. In summary, the synthesis framework implemented by $DS^2$ is highly effective in creating realistic delay spaces with compact $O(N)$ storage requirement.

## 5.4 Assumptions

$DS^2$ is designed based on a set of assumptions that are empirically derived from delays among edge networks in the Internet. It is not designed to synthesize delays within a local area network. Such a capability can be incorporated into $DS^2$ as future work.

We have experimented with PlanetLab delay data as well as P2PSim delay data and found that $DS^2$ can correctly synthesize the characteristics of these data sets. However, $DS^2$ may not work correctly on arbitrary delay data inputs that violate the following empirical assumptions:

• A low-dimensional Euclidean embedding can model the input delay data with reasonable accuracy, ignoring triangle inequality violations and local clustering properties. Some recent studies [21, 17] have shown that Euclidean embedding has difficulties in predicting pairwise Internet delays very accurately. Note, however, that we do not aim at predicting pairwise delays, we only use the Euclidean embedding as a compact model of the statistical properties of the input data.

• The in-degree distribution of the nearest neighbor graph computed from the input data is exponential. The current implementation of $DS^2$ automatically fits the in-degree distribution of the input data to an exponential distribution.

• The input data has a coarse-grained clustering structure. In addition, the delay edges across the same coarse-grained cluster pair exhibit similar triangle inequality violation characteristics.

## 6. APPLICATIONS

In this section, we demonstrate the importance of using a realistic delay model for simulation-based evaluation of distributed systems.

## 6.1 Server Selection

Increasingly, Internet services are distributed across multiple servers all over the world. The performance and cost of such Internet services depend on the server selection mechanisms they employ. Server selection redirects clients to an appropriate server, based on factors such as the location of the client, network conditions, and server load. A number of server selection systems [47, 11, 7] have been proposed and studied. In this section, the performance of Meridian [47], Vivaldi [7] and random server selection is evaluated using four different delay spaces: measured data, $DS^2$, Inet and GT-ITM.

We evaluate the accuracy of the three server selection algorithms using the delay penalty metric, which is defined as the difference between the delay to the chosen server and the delay to the closest server. We run each algorithm on all of the following data sets: for measured data, in addition to the full 3997-node data, we also use a 2k sample; for $DS^2$ data, we synthesize 2k data from a 1k sample of the measured data, and synthesize 4k and 16k data from a 2k

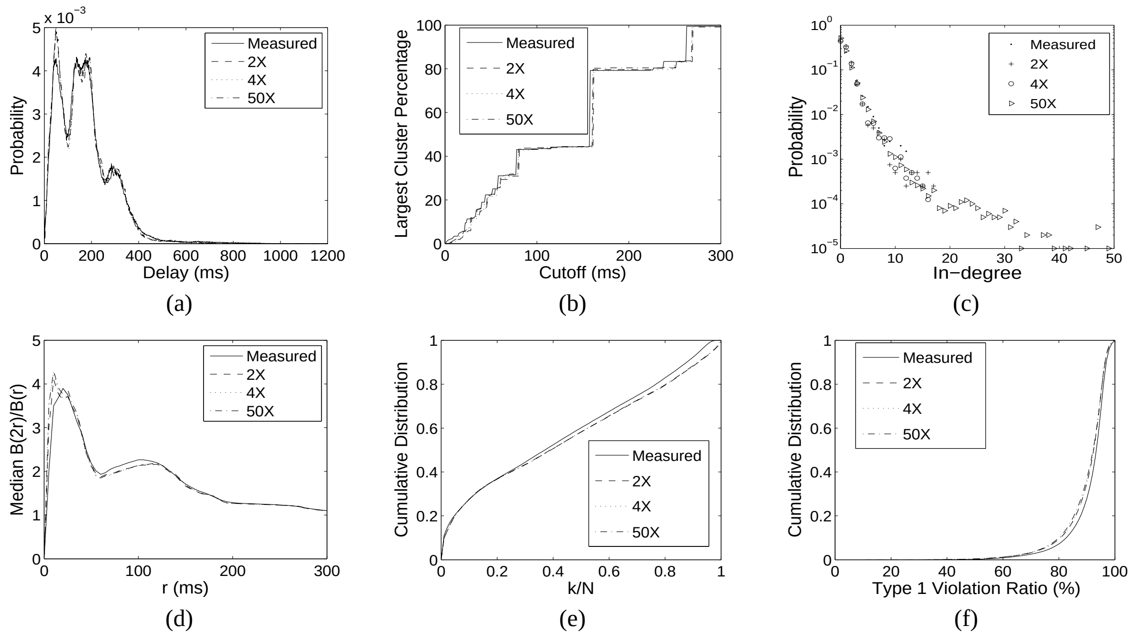

**Figure 13: $DS^2$ vs measured data. (a) Delay distribution. (b) Clustering cutoff. (c) In-degree distribution. (d) Median B(2r)/B(r). (e) D(k)/D(N). (f) Triangle inequality violation ratio distribution.**

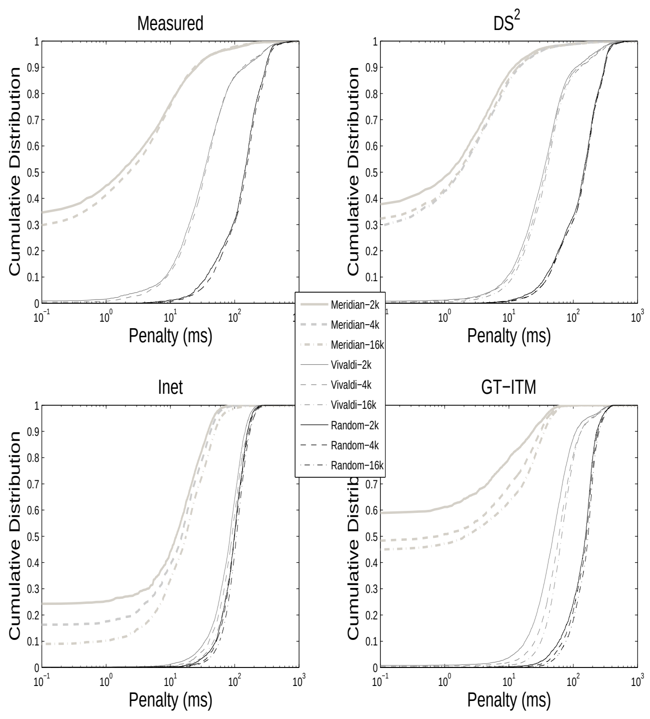

**Figure 14: Performance comparison of three server selection algorithms.**

sample of the measured data; for both Inet and GT-ITM, we generate 2k, 4k and 16k data sets, respectively, using the same methodology described in Section 2. In all server selection experiments, we assume that there is only one service available in the network, and all the nodes act as clients and servers simultaneously. Clients are not allowed to select themselves as their servers. For each data set, we run five experiments and the cumulative distributions of server selection penalties are presented in Figure 14.

First of all, the synthesized 2k and 4k $DS^2$ data sets yield virtually identical results as the 2k and 3997-node measured data, even though they are synthesized from only 1k and 2k measured data samples, respectively. Second, using the Inet delay model significantly underestimates the performance of Vivaldi. In fact, the results suggest that Vivaldi performs no better than random server selection, while Vivaldi performs much better than random selection if it is evaluated using the measured data or $DS^2$ data. Thus, using Inet as a delay model could lead to false conclusions about the performance of Vivaldi. Third, although the relative performance rank of the three algorithms is the same across all four delay models, the absolute performance estimated with Inet and GT-ITM differs dramatically from results achieved with the measured data or $DS^2$ data. For example, on the 3997-node measured data, 40.4% of the servers chosen by Meridian are within 1ms of the closest servers, while this number is 17.2% and 50.4% on 4k Inet and 4k GT-ITM data, respectively. Finally, the experiment based on the 16k $DS^2$ synthetic data indicates that the performance of Vivaldi should almost remain constant under scaling, but this is not the case with Inet and GT-ITM delay models. Similarly, Meridian's performance degrades more rapidly on Inet and GT-ITM than on $DS^2$ data with increasing network size. This illustrates that it is important to have good delay space models that are beyond our ability to measure since important performance trends sometimes only show at scale.

## 6.2 Structured Overlay Networks

Structured overlay networks like Chord, Kademlia and Pastry use proximity neighbor selection (PNS) to choose overlay neighbors [41, 23, 5]. PNS has been shown to effectively reduce routing stretch, query delay and network load, and to increase overlay robustness to failures and even to certain security attacks [37].

Here, we show the importance of using a good delay space to evaluate the effectiveness of PNS. To eliminate the influence of a particular PNS implementation, we assume in our simulations that the overlay chooses neighbors using perfect PNS, i.e., the closest node is chosen among all overlay nodes that satisfy the structural constraints imposed by a routing table entry. Unless otherwise stated, the results in this section have been evaluated on a 4000 node overlay network using FreePastry [12], where the delay space used was either based on measured data, $DS^2$, Inet, or GT-ITM.

We firstly evaluate the following metrics: *Overlay Indegree* of a node, which is the number of overlay nodes that have the node in their routing tables. *Hop Length Distribution* of overlay route, which determines the latency and network load of overlay lookups. *Route Convergence* of overlay routes, which, given two nodes located at distance $d$ from each other, measures what fraction of their overlay paths to a given destination is shared. This metric is important for dynamic caching and for the efficiency of multicast distribution trees.

Figure 15 shows that the results agree very well for the measured delay data and $DS^2$ data on all three metrics, while the results with the Inet and GT-ITM models differ significantly. The Inet model yields different results on indegree, because the power-law connectivity makes the closest leaf node of the high degree hubs in the topology the nearest neighbor for a large number of nodes. For the hop length distributions, we observe that the first hop of overlay routes with the Inet model is significantly larger than the first hop obtained with measured delay data. Finally, the route convergence with Inet/GT-ITM is higher than with the measured data. The deviations of these properties are rooted in the differences of the D(k)/D(N) growth metric and the local clustering in-degree metric among the delay models.

Next, we show how mis-predictions of the somewhat abstract overlay metrics shown above can have an impact on application performance metrics whose relevance is more immediately apparent.

**Effectiveness of PNS on Eclipse Attacks** - In recent work on defenses against Eclipse attacks [3] on structured overlay networks, Singh et al. [37] argue that PNS alone is a weak defense. While earlier work has shown that PNS is effective against Eclipse attacks based on simulations with a GT-ITM delay model [15], Singh et al. demonstrate that the defense breaks down when using measured delay data as a basis for simulations. Moreover, they show that the effectiveness of the defense diminishes with increasing size of the overlay network. We have repeated their simulations using $DS^2$ data and confirmed that the results match the simulations with measured data. Moreover, we are able to show that the effectiveness of PNS against Eclipse attacks continues to diminish as we increase the network size beyond the scale of measured delay data. This is another example of how the usage of inadequate delay models can lead to wrong conclusions. It also shows that $DS^2$ yields correct results, and that it is important to be able to synthesize delay models larger than measured data sets, in order to expose important trends.

**Performance of Proactive Replication** - The benefits of proactive replication in structured overlays to reduce overlay lookup hops and latency has been explored by Beehive [28]. We experimented with a simple prototype that does proactive replication based on the number of desired replicas of an object. The placement of replicas is biased towards nodes that share a longer prefix with the object identifier, in order to be able to intercept a large fraction of the overlay routes towards the home node of the object. We first evaluate the query lookup latency as a function of the total number of replicas for an object. Our system consists of a 4000 node network (3997 nodes for measured data) and a total of 10,000 objects.

Figure 16(a) shows that the average query latency for a given number of replicas is significantly lower with measured delay, especially when compared to Inet. This is an artifact of the different distributions of hop length as shown earlier in Figure 15(b). With the last hops in realistic models dominating the total overlay path, employing even a very few replicas results in reducing the average latency significantly. In the absence of realistic models, one would overestimate the number of replicas required to achieve a certain target lookup latency.

We then evaluate the distribution of query traffic to the replicas. In this scenario, we assume that the objects were replicated on all nodes that matched at least one digit with the object identifier. Given a network of 4000 nodes with Pastry node IDs as digits in base 16, we observe that this corresponds approximately to the expected value of $(1/16) * 4000 = 250$ replicas per object. Figure 16(b) shows the distribution of query load among the replicas. A point $(x, y)$ in the plot indicates that the $x$ lowest ranked nodes with respect to the amount of query traffic they served, together serve $y$% of the overall query traffic. The figure shows a huge imbalance in the load distribution for the Inet topology model, wherein 5% of the nodes serve over 50% of the traffic. This imbalance is caused due to the highly skewed overlay indegree distribution of nodes in the Inet topology.

Again, we see that the delay model used in simulations of distributed systems has a significant impact on the results obtained for important application performance metrics. Inadequate delay models can lead to false conclusions about the effectiveness and performance of systems.

## 7. RELATED WORK

Our work on modeling the Internet delay space is complementary to existing work on modeling network connectivity topologies. There is an opportunity for future work to incorporate delay space characteristics into topology models.

Early artificial network topologies had a straight-forward connectivity structure such as tree, star, or ring. A more sophisticated topology model that constructs node connectivity based on the random graph model was proposed by Waxman [45]. However, as the hierarchical nature of the Internet connectivity became apparent, solutions that more accurately model this hierarchy, such as Transit-Stub by Calvert *et al* [48] and Tier by Doar [8], emerged. Faloutsos *et al* [10] studied real Internet topology traces and discovered the power-law node degree distribution of the Internet. Li *et al* [18] further showed that router capacity constraints can be integrated with the power-law node degree model to create even more realistic router-level topologies.

There are many on-going projects actively collecting delay measurements of the Internet, including Skitter [38], AMP [2], PingER [27], and Surveyor [42] to name just a few examples. Some of these projects also collect one-way delays and hop-by-hop routing information. These projects typically use a set of monitoring nodes, ranging roughly from 20 to 100, to actively probe a set of destinations. The Skitter work probes on the order of 1 million destinations, which is the largest among these projects. The active monitoring method can probe any destination in the network, but the resulting measurements cover only a small subset of the delay space as observed by the monitors. Many of these measurements are also continuously collected, allowing the study of changes in delay over time. Our work uses the King tool to collect delay measurements, which restricts the probed nodes to be DNS servers, but

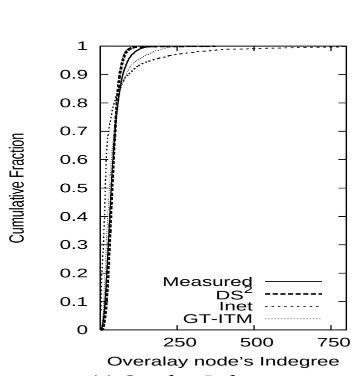

(a) Overlay Indegree

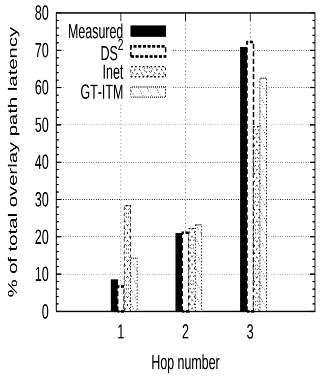

(b) Hop Length Distribution

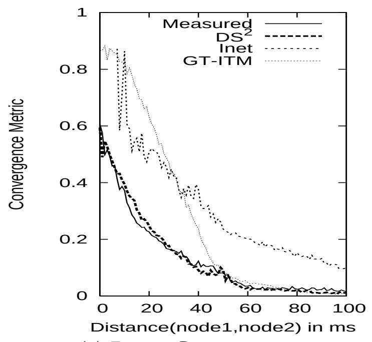

(c) Route Convergence

**Figure 15: Overlay properties.**

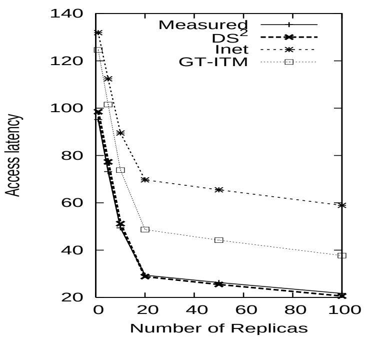

(a) Query latency

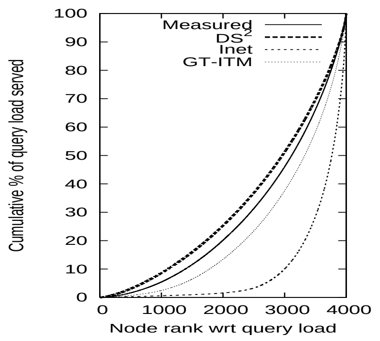

(b) Distribution of Query load

**Figure 16: Proactive replication.**

produces a symmetric delay space matrix, which lends itself to a study of the stationary delay space characteristics.

Some of the delay space properties reported in this paper have been observed in previous work. For example, triangle inequality violations and routing inefficiencies have been observed in [34] and [24]. Some of the characteristics of delay distributions and their implications for global clustering have been observed in Skitter. However, many of the observations made in this paper are new. These include the local clustering properties, and in particular the approximately exponential in-degree distribution, spatial growth properties, detailed properties of triangle inequality violations of different types and across different clusters, and the examination of these properties under scaling. In addition to the "static" properties of delay, previous work have also studied the temporal properties of Internet delay [1]. Incorporating temporal properties into a delay space model is an area for future work.

One key technique used in our work is computing a low dimensional Euclidean embedding of the delay space to enhance the completeness and scalability of the delay space representation. Many approaches for computing such an embedding have been studied [24, 7, 35, 6, 19, 43, 36, 26]. We have not considered the impact of using different computation methods or using different embedding objective functions. This represents another area for future work.

## 8. CONCLUSIONS

To the best of our knowledge, this is the first study to systematically analyze, model, and synthesize the Internet delay space. We quantify the properties of the Internet delay space with respect to a set of metrics relevant to distributed systems design. This leads to new understandings of the Internet delay space characteristics which may inform future work. We also develop a set of building block techniques to model and synthesize the Internet delay space compactly while accurately preserving all relevant metrics. The result is an Internet delay space synthesizer called $DS^2$ that can produce realistic delay spaces at large scale. $DS^2$ requires only $O(N)$ memory, where $N$ is the number of nodes, and requires only simple run-time calculations to generate the delay between a pair of nodes. This helps to address the memory requirement barrier of conducting large-scale simulations. $DS^2$ provides an important mechanism for simulating and emulating distributed systems at large-scale, which complements other evaluation methodologies. See [9] for further information on $DS^2$.

## Acknowledgment

We would like to thank Atul Singh for providing the results for the Eclipse attack experiments, and Evan Stade for providing a simulator of Meridian. We also thank the anonymous reviewers for their valuable feedback.

## 9. REFERENCES

[1] A. Acharya and J. Saltz. A Study of Internet Round-Trip Delay. Technical Report CS-TR-3736, University of Maryland, College Park, 1996.
[2] Active measurement project, NLANR. http://watt.nlanr.net.

[3] M. Castro, P. Druschel, A. Ganesh, A. Rowstron, and D.S. Wallach. Security for structured peer-to-peer overlay networks. In *Proceedings of OSDI*, Boston, MA, December 2002.

[4] Miguel Castro, Peter Druschel, Y. Charlie Hu, and Antony Rowstron. Exploiting network proximity in peer-to-peer overlay networks. Technical Report MSR-TR-2002-82, Microsoft Research, May 2002.

[5] Miguel Castro, Peter Druschel, Y. Charlie Hu, and Antony Rowstron. Proximity neighbor selection in tree-based structured peer-to-peer overlays. Technical Report MSR-TR-2003-52, Microsoft Research, June 2003.

[6] M. Costa, M. Castro, A. Rowstron, and P. Key. PIC: Practical Internet coordinates for distance estimation. Technical Report MSR-TR-2003-53, Microsoft Research, September 2003.

[7] F. Dabek, R. Cox, F. Kaashoek, and R. Morris. Vivaldi: A decentralized network coordinate system. In *Proceeding of ACM SIGCOMM*, August 2004.

[8] M. Doar. A better model for generating test networks. In *Proceeding of IEEE GLOBECOM*, November 1996.

[9] $DS^2$. http://www.cs.rice.edu/$\sim$eugeneng/research/ds2/.

[10] C. Faloutsos, M. Faloutsos, and P. Faloutsos. On Power-law Relationships of the Internet Topology. In *Proceedings of ACM Sigcomm*, August 1999.

[11] Michael J. Freedman, Karthik Lakshminarayanan, and David Mazieres. Oasis: Anycast for any service. In *Proceedings of ACM NSDI*, May 2006.

[12] Freepastry. http://freepastry.rice.edu/.

[13] K. P. Gummadi, S. Saroiu, and S. D. Gribble. King: Estimating latency between arbitrary internet end hosts. In *Proceedings of the SIGCOMM IMW*, Marseille, France, November 2002.

[14] Krishna P. Gummadi, Ramakrishna Gummadi, Steven D. Gribble, Sylvia Ratnasamy, Scott Shenker, and Ion Stoica. The impact of DHT routing geometry on resilience and proximity. In *Proc. ACM SIGCOMM*, Karlsruhe, Germany, August 2003.

[15] K. Hildrum and J. Kubiatowicz. Assymtotically efficient approaches to fault tolerance in peer-to-peer networks. In *Proc. 17th International Symposium on Distributed Computing*, Sorrento, Italy, Oct 2003.

[16] David R. Karger and Matthias Ruhl. Finding nearest neighbors in growth restricted metrics. In *Proccedings of ACM Symposium on Theory of Computing*, 2002.

[17] Sanghwan Lee, Zhi-Li Zhang, Sambit Sahu, and Debanjan Saha. On suitability of Euclidean embedding of Internet hosts. In *Proc. SIGMETRICS 2006*, June 2006.

[18] L. Li, D. Alderson, W. Willinger, and J. Doyle. A first-principles approach to understanding the internet's router-level topology. In *Proceeding of ACM SIGCOMM*, August 2004.

[19] H. Lim, J. Hou, and C.-H. Choi. Constructing internet coordinate system based on delay measurement. In *Proceedings of IMC*, Miami, FL, October 2003.

[20] Jesper Møller and Rasmus Waagepetersen. *Statistical Inference and Simulation for Spatial Point Processes*. Chapman and Hall/CRC, 2004.

[21] Eng Keong Lua, Timothy Griffin, Marcelo Pias, Han Zheng, and Jon Crowcroft. On the accuracy of embeddings for internet coordinate systems. In *Proceedings of IMC*, Berkeley, CA, October 2005.

[22] Harsha V. Madhyastha, Tomas Isdal, Michael Piatek, Colin Dixon, Thomas Anderson, Arvind Krishnamurthy, and Arun Venkataramani. iPlane: an information plane for distributed services. In *Proc. OSDI 2006*, November 2006.

[23] P. Maymounkov and D. Mazieres. Kademlia: A peer-to-peer information system based on the xor metric. In *Proc. IPTPS 2002*, March 2002.

[24] T. S. E. Ng and H. Zhang. Predicting Internet networking distance with coordinates-based approaches. In *Proceedings of IEEE INFOCOM*, June 2002.

[25] p2psim. http://www.pdos.lcs.mit.edu/p2psim/.

[26] M. Pias, J. Crowcroft, S. Wilbur, T. Harris, and S. Bhatti. Lighthouses for scalable distributed location. In *Proceedings of IPTPS*, 2003.

[27] PingER. http://www.slac.stanford.edu/comp/net/wan-mon/tutorial.html.

[28] V. Ramasubramanian and E.G Sirer. Beehive: O(1) lookup performance for pwer-law query distributions in peer-to-peer overlays. In *Proc. NSDI '04*, San Francisco, California, March 2004.

[29] S. Ranjan, R. Karrer, and E. Knightly. Wide area redirection of dynamic content by internet data centers. In *Proceedings of IEEE INFOCOM*, Hong Kong, China, 2004.

[30] S. Ratnasamy, S. Shenker, and I. Stoica. Routing algorithms for DHTs: Some open questions. In *Proceedings of IPTPS*, Cambridge, MA, March 2002.

[31] Rolf-Dieter Reiss. *A Course on Point Processes*. Springer Series in Statistics. Springer, 1993.

[32] Route views. http://www.routeviews.org/.

[33] B. Bhattacharjee S. Banerjee and C. Kommareddy. Scalable Application Layer Multicast. In *Proceedings of ACM SIGCOMM*, August 2002.

[34] S. Savage, A. Collins, E. Hoffman, J. Snell, and T. Anderson. The End-to-end Effects of Internet Path Selection. In *Proceedings of ACM Sigcomm*, August 1999.

[35] Y. Shavitt and T. Tankel. Big-bang simulation for embedding network distances in Euclidean space. In *Proceedings of IEEE INFOCOM*, San Francisco, CA, March 2003.

[36] Y. Shavitt and T. Tankel. On the curvature of the Internet and its usage for overlay construction and distance estimation. In *Proceedings of IEEE INFOCOM*, April 2004.

[37] A. Singh, T. W. Ngan, P. Druschel, and D. S. Wallach. Eclipse attacks on overlay networks: Threats and defenses. In *Proc. INFOCOM 2006*, Barcelona, Spain, April 2006.

[38] Skitter. http://www.caida.org/tools/measurement/skitter/.

[39] A. Slivkins. Distributed Approaches to Triangulation and Embedding. In *Proceedings 16th ACM-SIAM Symposium on Discrete Algorithms (SODA)*, 2004.

[40] A. Slivkins, J. Kleinberg, and T. Wexler. Triangulation and Embedding using Small Sets of Beacons. In *Proceedings of FOCS*, 2004.

[41] I. Stoica, R. Morris, D. Karger, M. F. Kaashoek, and H. Balakrishnan. Chord: A scalable peer-to-peer lookup service for Internet applications. In *Proceedings of ACM SIGCOMM*, 2001.

[42] Surveyor. http://www.advanced.org/csg-ippm/.

[43] L. Tang and M. Crovella. Virtual landmarks for the internet. In *Proceedings of IMC*, Miami, FL, October 2003.

[44] Marcel Waldvogel and Roberto Rinaldi. Efficient Topology-Aware Overlay Network. In *First Workshop on Hot Topics in networks (HotNets-I)*, October 2002.

[45] B. Waxman. Routing of multipoint connections. *IEEE J. Select. Areas Commun.*, December 1988.

[46] J. Winick and S. Jamin. Inet-3.0: Internet topology generator. Technical Report UM-CSE-TR-456-02, University of Michigan, 2002.

[47] Bernard Wong, Aleksandrs Slivkins, and Emin Gun Sirer. Meridian: A lightweight network location service without virtual coordinates. In *Proceedings of ACM SIGCOMM*, August 2005.

[48] E. W. Zegura, K. L. Calvert, and S. Bhattacharjee. How to Model an Internetwork. In *Proceedings of IEEE INFOCOM*, March 1996.

[49] B. Zhao, J. Kubiatowicz, and A. Joseph. Tapestry: An infrastructure for wide-area fault-tolerant location and routing. *U.C. Berkeley Technical Report UCB//CSD-01-1141*, 2001.